The current issue and full text archive of this journal is available at
www.emeraldinsight.com/0961-5539.htm

A numerical heat transfer study of slot jet impinging on an inclined plate

Ahad Ramezanpour
Faculty of Science and Technology, Anglia Ruskin University, Chelmsford, UK
Iraj Mirzaee
Faculty of Engineering, Urmia University, Urmia, Iran
David Firth
Research and Development Services, Anglia Ruskin University, Chelmsford, UK, and
Hassan Shirvani
Faculty of Science and Technology, Anglia Ruskin University, Chelmsford, UK

Received 23 March 2005
Revised 30 June 2006
Accepted 15 November 2006

Abstract

Purpose – This paper seeks to conduct a numerical study to investigate heat transfer in turbulent, unconfined, submerged, and inclined impinging jet discharged from a slot nozzle, utilising finite volume code FLUENT.

Design/methodology/approach – Two re-normalisation group k-ε and the basic Reynolds stress models by using enhanced wall treatment for near wall turbulent modelling were applied and the local Nusselt numbers were compared with experiments. The enhanced wall treatment solves the fully turbulent region and viscous sublayer by considering a single blended function of both layers.

Findings – In inclined impinging jet by movement of stagnation point to the uphill side of the impinging plate, the location of the maximum Nusselt number moves to the uphill side of the plate. However, this movement increases by increasing of H/D and by decreasing of Reynolds number and inclination angle. For a flat plate impinging jet, the results were found to be less than 8 per cent different and for inclined impinging jet, more sensitive to H/D, 5-20 per cent different in comparison with experiments. In addition, the flow streamlines were consistent with location of the heat transfer peak on the impinging surface.

Research limitations/implications – Reynolds numbers in range of 4,000-16,000, the ratio of nozzle height to hydraulic diameter of the nozzle (H/D) in range of 4-10, and inclination angle of air jet and plate in range of 40-90° were considered.

Originality/value – A unique achievement of this study in comparison with experimental data was locating the exact peak of the local Nusselt number on impinging plate by change of Reynolds number, H/D, and inclination angle.

Keywords Heat transfer, Turbulent flow, Fluid phenomena, Jets

Paper type Research paper

Nomenclature

$C^*_{2\varepsilon}$ = modified constant in ε equation
c_p = specific heat in constant pressure
d_{ij} = diffusion of Reynolds stresses
D = hydraulic diameter of slot nozzle
G_k = turbulent energy generation rate
h = convection heat transfer coefficient
H = nozzle exit-to-plate distance

International Journal of Numerical Methods for Heat & Fluid Flow
Vol. 17 No. 7, 2007
pp. 661-676

0961-5539
DOI 10.1108/09615530710777949

k = turbulence kinetic energy
n_i = x_i component unit normal to wall
Nu = Nusselt number (hD/λ)
p = pressure
P_{ij} = Reynolds stress generation rate
Pr = molecular Prandtl number
Pr_k = Prandtl number for k
Re = Reynolds number ($\rho UD/\mu$)
S = strain rate
S_{ij} = mean strain tensor
T = temperature
T^+ = dimensionless thermal wall parameter
u^+ = dimensionless near wall velocity
u_i = Cartesian velocity component
U = fluid mean velocity at nozzle exit
$\overline{u_i u_j}$ = Reynolds stresses
x_i = spatial coordinate
y = vertical distance from wall
y^+ = dimensionless wall parameter

Greek symbols

Γ,Π = near wall blending functions
δ_{ij} = Kronecker delta
ε = turbulence dissipation rate
ε_{ij} = dissipation rate of Reynolds stresses
η = Sk/ε
θ = impinging jet inclination angle
κ = Von Karman constant
λ = conduction coefficient
μ = viscosity
μ_t = eddy viscosity
ρ = density
ϕ_{ij} = pressure strain correlation
ϕ_{ij}^1 = slow (turbulence) pressure strain
ϕ_j^2 = rapid (mean shear) pressure strain
ϕ_{ij}^w = wall reflection pressure strain

1. Introduction

Impinging jets have received considerable attention because of the high heat/mass transfer rates in the impinging region which leads to applications in heating, cooling, drying and materials processing. Direct and localised cooling in addition to high heat transfer rates makes impinging jets suitable for the thermal management of electronic equipments. Using the inclined jet helps flexible electronic packaging design, grants the required removal heat rate, and also can be used as a ventilation tool by guiding the coolant fluid.

The experimental studies in impinging jets have sometimes been contradictory because of differences in the conditions of experiments such as geometry, inlet turbulence and inlet velocity profile. The results of the present numerical study for slot nozzle, inclined, unconfined, and submerged impinging jet are compared with the experimental work of Beitelmal *et al.* (2000).

The study by Obot *et al.* (1982) concluded that confinement reduces the heat transfer rate from 5 to 10 per cent when $H/D < 12$. The entrainment of ambient air and pressure distribution are the two main parameters which affect confinement of the submerged impinging jets (Saad *et al.*, 1992). In comparison, slot nozzle impinging jets results in an even distribution of heat transfer coefficient while round jet nozzles give higher heat transfer rates in stagnation regions. Baughn and Shimizu (1989), Lytle and Webb (1994), and Yung-Yang *et al.*(1997) experimentally studied the effect of various values of H/D, Reynolds number, and amount of heat flux from the impinging plate on local heat transfer rate. Moreover, experimental research by Royne and Dey (2006) studied pressure drop and heat transfer for dissimilar nozzle geometries of impinging jet arrays.

The effect of inclination has been studied by Beltaos (1976), Stevens and Webb (1991) and Yan and Saniei (1997). Beitelmal *et al.* (2000) concluded that the maximum heat transfer region in inclined slot jet shifts towards the uphill side of the plate and the maximum Nusselt number value decreases as the inclination

angle decreases. Also heat transfer distribution in the uphill side becomes less sensitive to the magnitude of H/D.

Craft *et al.* (1993) compared the low Reynolds k-ε model, the basic Reynolds stress model, and two modified Reynolds stress models. The results of the first two cases achieved poor agreement while modification in wall reflection pressure strain of Reynolds stress model improved accuracy of the numerical simulation.

Durbin (1996) concluded that the growth of turbulent kinetic energy in standard k-ε model in the stagnation region causes an overestimation of the heat transfer rate. Behnia *et al.* (1996) improved the Nusselt number prediction by using the $v2f$ model of Durbin (1995). The other study by Behnia *et al.* (1999) using $v2f$ model compared confined and unconfined impinging jets and showed that confinement decreases the average heat transfer rate; however the local stagnation heat transfer rate remains constant.

Morris *et al.* (1999) by using commercial code FLUENT achieved a good agreement in the flow pattern of the confined impinging jet by Reynolds stress model and poor prediction by standard and re-normalisation group (RNG) k-ε models and using wall function for near wall turbulence modelling.

Park and Sung (2001) obtained good prediction of the local heat transfer rate for a round nozzle flat plate impinging jet by modifying the near wall conditions of the k-ε-f_μ model. The numerical flow and heat transfer study of a confined slot nozzle impinging jet by using the k-w turbulent model was reported by Park *et al.* (2003) and showed satisfactory agreement of the local Nusselt number in comparison with experiments; but the agreement on the second peak of heat transfer rate was reduced by increase of Reynolds number to 25,000. Furthermore, a comprehensive paper review and experimental study on near wall trends of velocity, temperature and turbulent intensity and evaluation of logarithmic wall law was carried out by Guerra *et al.* (2005).

Roy and Patel (2003) applied the RNG k-ε model and wall function by using FLUENT for three dimensional two pairs of inclined rectangular nozzles and discussed flow-thermal characteristics of the results without comparison with experimental data. A three-dimensional numerical flow field and heat transfer rate study of an inclined jet with cross flow by using the standard k-ε model and wall function was carried out by Yue-Tzu and Yong-Xun (2005). The study considered a fixed $Re = 5{,}000$ and an inclination angle of 45°. However, the comparison of the Nusselt number with experiments showed a considerable difference on the impinging area.

The mixed convection effect on flow and heat transfer rate of a slot nozzle impinging jet in a laminar regime was investigated by Sahoo and Sharif (2004). The results showed no significant effect on the total Nusselt number for dissimilar Richardson numbers.

In heat transfer study of an impinging jet, the near wall turbulence modelling is an important parameter because most of temperature drop happens across the low Reynolds number sub-layer (Craft *et al.*, 1993). Note that the heat transfer rate also depends on the level of turbulence energy prevailing near the edge of the fully turbulent region and thus is quite sensitive to the type of turbulence model.

This study compares the Reynolds stress and RNG k-ε models by using enhanced wall treatment for near wall turbulence modelling by commercial code FLUENT 6.0 and for a slot nozzle impinging jet on the flat and inclined plates. Enhanced wall treatment solves the turbulence sublayer instead of using function to set and simulate

turbulence behaviour near the wall. The heat transfer on the impinging plate has been studied for various Reynolds numbers, H/D, and inclination angles for both aforementioned turbulence models and compared with experimental results.

2. Numerical modelling

2.1 Governing equations

The Navier-Stokes equations for incompressible flow, constant fluid properties and steady state condition may be written as:

$$\begin{aligned} &\frac{\partial u_i}{\partial x_i} = 0 \quad \text{continuity equation,} \\ &\rho u_j \frac{\partial u_i}{\partial x_j} = -\frac{\partial p}{\partial x_i} + \mu \frac{\partial^2 u_i}{\partial x_j^2} \quad \text{momentum equation,} \\ &\rho c_p u_i \frac{\partial T}{\partial x_i} = \lambda \frac{\partial^2 T}{\partial x_i^2} \quad \text{energy equation} \end{aligned} \tag{1}$$

2.2 RNG k-ε *turbulence modelling*

For modelling the Reynolds transports in averaged form of Navier-Stokes equations, two transport equations for RNG k-ε model for turbulence kinetic energy (k) and its dissipation rate (ε), respectively, are used as:

$$\begin{aligned} \rho u_i \frac{\partial k}{\partial x_i} &= \frac{\partial}{\partial x_j}\left(\left(\mu + \frac{\mu_t}{Pr_t}\right)\frac{\partial k}{\partial x_j}\right) + G_k - \rho\varepsilon, \\ \rho u_i \frac{\partial \varepsilon}{\partial x_i} &= \frac{\partial}{\partial x_j}\left(\left(\mu + \frac{\mu_t}{Pr_t}\right)\frac{\partial \varepsilon}{\partial x_j}\right) + C_{1\varepsilon}\frac{\varepsilon}{k} G_k - C_{2\varepsilon}^* \rho \frac{\varepsilon^2}{k} \end{aligned} \tag{2}$$

where G_k (turbulence energy generation) $= 2\mu_t S_{ij} \frac{\partial u_j}{\partial x_i}$

In the above equations, the right-hand side involves diffusion, generation and dissipation rate terms and left-hand side is convection term. The turbulence viscosity is modelled as $\mu_t = C_\mu \rho k^2/\varepsilon$ where from RNG theory $C_\mu = 0.0845$. The turbulent Prandtl number is calculated from an algebraic equation and/which was derived form RNG theory (Fluent, 2005). Also $C_{1\varepsilon} = 1.42$ and $C_{2\varepsilon}^*$ is calculated from:

$$C_{2\varepsilon}^* = C_{2\varepsilon} + \frac{C_\mu \rho \eta^3 (1 - \eta/\eta_0)}{1 + \beta\eta^3} \tag{3}$$

where $C_{2\varepsilon} = 1.68$, $\beta = 0.012$, $\eta_0 = 4.38$, and $\eta = Sk/\varepsilon$. In the low-strain region ($\eta < \eta_0$), the effect of equation (3) is to increase $C_{2\varepsilon}$ and the result is comparable to standard k-ε model. In the high-strain region ($\eta > \eta_0$), the equation (3) leads to a reduction of $C_{2\varepsilon}$. The less destruction of ε augments dissipation and reduces the kinetic energy and effective viscosity. This improves the prediction of heat transfer in the impinging (high-strain) region by the RNG k-ε model compared to the standard k-ε model that overestimates the kinetic energy and heat transfer rate in the impinging region (Durbin, 1996).

2.3 Reynolds stress turbulence modelling

The transport equations of the basic Reynolds stress model may be written as:

$$\rho u_k \frac{\partial\left(\overline{u_i u_j}\right)}{\partial x_k} = d_{ij} + P_{ij} + \phi_{ij} + \varepsilon_{ij} \tag{4}$$

where the right-hand side is diffusion, generation, pressure strain, and dissipation terms, respectively, and the left-hand side is convection term. The diffusion, generation and dissipation terms are obtained from:

$$\begin{aligned} d_{ij} &= \frac{\partial}{\partial x_k}\left(\frac{\mu_t}{Pr_k}\frac{\partial\left(\overline{u_i u_j}\right)}{\partial x_k}\right), \\ P_{ij} &= -\rho\left(\overline{u_i u_k}\frac{\partial u_j}{\partial x_k} + \overline{u_j u_k}\frac{\partial u_i}{\partial x_k}\right), \\ \varepsilon_{ij} &= \frac{2}{3}\rho\delta_{ij}\varepsilon \end{aligned} \tag{5}$$

where in diffusion term, $\mu_t = \rho C_{\mu,\mathrm{RS}} k^2/\varepsilon$ and the constants are $C_{\mu,\mathrm{RS}} = 0.09$ and $Pr_k = 0.82$. The pressure strain term in equation (4) is obtained from:

$$\phi_{ij} = \phi_{ij}^1 + \phi_{ij}^2 + \phi_{ij}^w,$$

where

$$\begin{aligned} \phi_{ij}^1 &= -c_1\rho\frac{\varepsilon}{k}\left(\overline{u_i u_j} - \frac{2}{3}\delta_{ij}k\right) \\ \phi_{ij}^2 &= -c_2\left(P_{ij} - \frac{1}{3}\delta_{ij}P_{kk}\right) \\ \phi_{ij}^w &= c_{1w}\frac{\varepsilon}{k}\left(\overline{u_k u_m}n_k n_m\delta_{ij} - \frac{3}{2}\overline{u_i u_k}n_i n_k\delta_{ij} - \frac{3}{2}\overline{u_j u_k}n_j n_k\delta_{ij}\right)\frac{k^{3/2}}{c_l\varepsilon y} \\ &\quad + c_{2w}\left(\phi_{km}^2 n_k n_m\delta_{ij} - \frac{3}{2}\phi_{ik}^2 n_i n_k\delta_{ij} - \frac{3}{2}\phi_{jk}^2 n_j n_k\delta_{ij}\right)\frac{k^{3/2}}{c_l\varepsilon y} \end{aligned} \tag{6}$$

where n_i is the x_i component of the unit normal to the wall and y is the normal distance to the wall. The constants of the strain rate term are $c_1 = 1.8$, $c_2 = 0.6$, $c_{1w} = 0.5$, $c_{2w} = 0.3$, and $c_l = C_{\mu,\mathrm{RS}}^{3/4}/k$, where $\kappa = 0.4187$ is von Karman constant.

The scalar dissipation rate, ε in equations (5) and (6), is computed by the transport equation of dissipation rate for the standard k-ε model as:

$$\rho u_i \frac{\partial\varepsilon}{\partial x_i} = \frac{\partial}{\partial x_i}\left[\left(\mu + \frac{\mu_t}{Pr_k}\right)\frac{\partial\varepsilon}{\partial x_i}\right] + \frac{1}{2}C_{\varepsilon 1}P_{ii} - C_{\varepsilon 2}\rho\frac{\varepsilon^2}{k} \tag{7}$$

where the constants are $Pr_k = 1.0$, $C_{\varepsilon 1} = 1.44$, and $C_{\varepsilon 2} = 1.92$.

2.4 Near wall turbulence modelling

Both the RNG k-ε and basic Reynolds stress models applied in this study use enhanced wall treatment for near wall turbulence modelling. In this model, the momentum and k

equations for the inner region ($Re_y = \rho y\sqrt{k}/\mu < 200$) are solved and eddy viscosity as well as dissipation rate is obtained algebraically. In the inner region, the eddy viscosity and dissipation rate are calculated based on a blending function in which its output near the wall leads to the algebraic values of a one-equation turbulence model and in boundaries of the outer region ($Re_y = 200$) leads to the values of the turbulence model to be solved in the outer region (Fluent, 2005).

The temperature and velocity near the wall are obtained by blending the laminar linear sublayer and turbulence logarithmic laws (Kader, 1981):

$$\begin{aligned} u^+ &= e^{\Gamma} u^+_{\text{lam}} + e^{1/\Gamma} u^+_{\text{turb}}, \\ \frac{\mathrm{d}u^+}{\mathrm{d}y^+} &= e^{\Gamma} \frac{\mathrm{d}u^+_{\text{lam}}}{\mathrm{d}y^+} + e^{1/\Gamma} \frac{\mathrm{d}u^+_{\text{turb}}}{\mathrm{d}y^+} \end{aligned} \tag{8}$$

where

$$\Gamma = -\frac{a(y^+)^4}{1 + by^+}$$

$$T^+ = e^{\Pi} T^+_{\text{lam}} + e^{1/\Pi} T^+_{\text{turb}}$$

where

$$\Pi = -\frac{a(Pr\, y^+)^4}{1 + b\, Pr^3 y^+} \tag{9}$$

where $a = 0.01$, $b = 5.0$, and $\kappa = 0.41$ is von Karman constant. The generation term when solving the k equation near the wall is obtained using equations (8).

2.5 Computational domain

2.5.1 Computational domain geometry. The two dimensional computational domain consists of the inlet, impinging wall, nozzle walls, and outlet boundaries (Figure 1). The inclined impinging jet is studied by rotating the flat plate around a fixed symmetry point and the nozzle-exit-to-plate ratio is based on the distance of the nozzle from the fixed point on the plate. The nozzle length is 5.5 mm, and the impinging heated plate length is 0.2 m similar to the experimental setup. In the impinging region, to prevent the influence of the outlet boundary conditions on the flow and heat transfer, the impinging wall was extended to 0.9 m without heat flux. Similarly, the height of the outlet boundary condition was set to 1 m. The outlet boundary condition was found to be more sensitive in the Reynolds stress turbulence model, causing reduction of the heat transfer rate in the stagnation region when the boundary was not far enough to satisfy zero diffusion flux.

2.5.2 Boundary conditions.

2.5.2.1 Inlet. To set a parabolic velocity profile and turbulent values at nozzle exit, a two dimensional duct flow with a fixed length was solved numerically and the outlet velocity profile, turbulence intensity, and turbulence length scale were adjusted as inlet conditions of impinging jet domain. The turbulence intensity in the inlet of the duct was set at 2 per cent and the turbulence length scale based on the hydraulic diameter of duct was set to 0.001 m. The length of duct was fixed to 0.2 m which, in

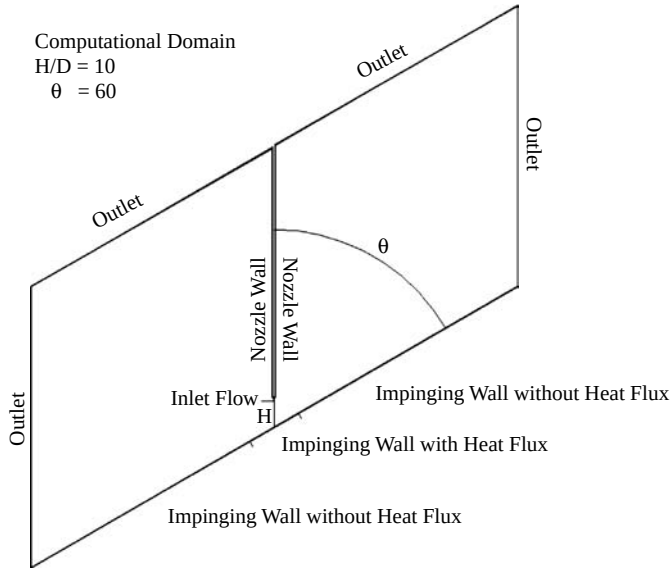

Figure 1.
Computational domain of inclined impinging jet

range of Reynolds number in this study, leads to a fully developed parabolic velocity profile in the outlet of duct.

2.5.2.2 Walls. The velocity field on the walls complied with no-slip conditions. The heat flux in the heated impinging region was set to 100 W/m^2.

2.5.2.3 Outlet. The outlet boundary condition was set to a constant atmospheric pressure and the associated parameters were obtained by assuming zero diffusion flux.

The working fluid in this study was incompressible air with constant properties due to less than 10 K temperature difference in the domain.

2.5.3 Grid considerations. Using the enhanced wall treatment to solve the viscous sublayer demands a fine grid size perpendicular to the wall. Figure 2 shows a sample grid which was used in this study. A boundary layer grid of 24 rows was applied to the impinging wall where the height of the first row was set to 10^{-5} m and the growing factor

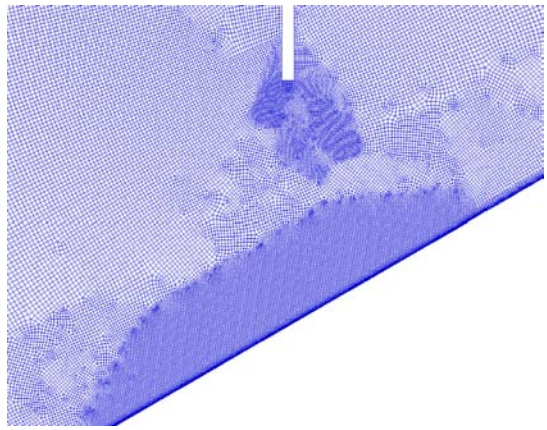

Figure 2.
The grid sample used between nozzle and inclined plates

of boundary layer grid height adjusted to 1.2. The number of grids parallel to the wall in the heated region was set to 200. Two grid independency tests were used by changing the grid sizes parallel and vertical to the wall. The grid independency test was carried out by the RNG k-ε model and for a flat plate impinging jet of $H/D = 6$ and $Re = 4{,}000$. Detailed information of grid tests and their effect on the Nusselt number is given in Tables I and II.

Increasing of number of grids parallel to the wall from 100 to 300 changed the Nusselt number by less than 2.5 per cent and the solution was assumed grid independent.

For capturing a laminar viscous sublayer, the non-dimensional wall coordinate (y^+) is recommended to be equal to 1 at the wall-adjacent cells (Fluent, 2005). The wall coordinate is given by:

$$y^+ = \frac{\rho C_{\mu,\text{wall}}^{1/4} k^{1/2} y}{\mu} \tag{10}$$

Here, y is the distance from the wall, k is the turbulence kinetic energy, $C_{\mu,\text{wall}} = 0.09$, and ρ, μ are density and viscosity. The data in Table II confirms that by using enhanced wall treatment for impinging jet modelling in the stagnation-adjacent cell, y^+ should be about 0.5. The Nusselt number along the impinging wall for different conditions of Table II shows that the y^+ above the critical value leads to incorrect prediction. The effect of exceeding y^+ from the critical point is shown in the stagnation region of Figure 3. Below the critical y^+ changing the grid height from 5×10^{-6} to 10^{-4} m showed a change in stagnation Nusselt number of 5 per cent which can be assumed grid independent.

2.6 Solution parameters

A segregated and explicit solver was utilised to solve the flow, energy, turbulence and the Reynolds stress (for Reynolds stress model) equations. For the pressure-velocity coupling SIMPLE algorithm was used whilst PRESTO! (PREssure STaggering Option) was applied for the pressure discretization, which is suitable for steep pressure gradients. The momentum and Reynolds stress equations were discretized by the second order interpolation scheme because of rotational flow crossing the grids. The common value of under-relaxation factors for pressure was set to 0.2 for the

Table I.
Grid independency test detail parallel to wall

Grid number parallel to wall in heat flux region	Stagnation Nusselt number	Stagnation-adjacent cell (y^+)
100	31.05	0.066
200	30.42	0.044
300	30.31	0.035

Table II.
Grid independency test detail vertical to wall

B.L. grid first row size (m)	B.L. grid growing factor	B.L. grid number of rows	Stagnation Nusselt number	Stagnation-adjacent cell (y^+)
5×10^{-6}	1.2	36	30.42	0.02
1×10^{-5}	1.2	24	30.97	0.044
1×10^{-4}	1.15	16	32.03	0.447
5×10^{-4}	1.15	10	–	1.71

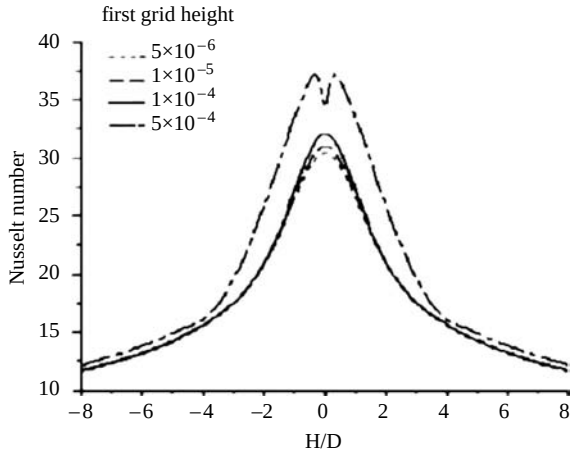

Figure 3.
Local Nusselt number on the impinging wall with different sizes of first boundary layer grid height (Table II)

Reynolds stress and 0.3 for the RNG k-ε model while other parameters were set to 0.4 for Reynolds stress and 0.6 for the RNG k-ε model.

The Reynolds stress model cases were initialized by the solution of the RNG k-ε model. In each case, the solution was considered converged when the normalized and scaled residual errors were reduced to 10^{-4} for continuity, momentum, and turbulence and 10^{-6} for energy equations.

3. Results and discussion

In the impinging jet, flow along the centre line of the nozzle to stagnation point on the plate and its vicinity is almost irrotational with rapid normal strain changes. In contrast, the outer periphery of impinging jet, flow is strongly rotational and with stream line curvature. However, from the vicinity of the stagnation point on the wall, changes from normal to shear stresses take place along the wall.

In the slot nozzle flat plate impinging jet, the maximum Nusselt number on the impinging plate happens at the stagnation point and the Nusselt number reduces along the wall in the direction of flow. The value of the Nusselt number in the ranges studied, increases by reduction of the H/D and increasing Reynolds number.

With the impinging jet on an inclined plate, the maximum Nusselt number occurs at an uphill position of the plate similar to the stagnation point. This can qualitatively be described by dividing the velocity vector from the nozzle exit to two components of parallel and vertical to the plate, the parallel component acts as a wall jet in the downhill side of the plate and the vertical component causes creation of a stagnation point which is on the uphill side of the plate. Figure 4 shows the streamlines of an impinging jet to flat and inclined plates ($H/D = 10$, $Re = 12{,}000$, $\theta = 40$, 60, and 90) by using the Reynolds stress model and one case of $\theta = 40$ by applying the RNG k-ε model. The RNG k-ε eddy viscosity model assumes an isotropic (linear) change in Reynolds stresses with strain tensor however, the Reynolds stress model takes into account non-isotropic turbulence effects and solves each of the Reynolds stresses hence gives more accurate prediction of streamlines by showing creation of recirculating flow (Morris *et al.*, 1999).

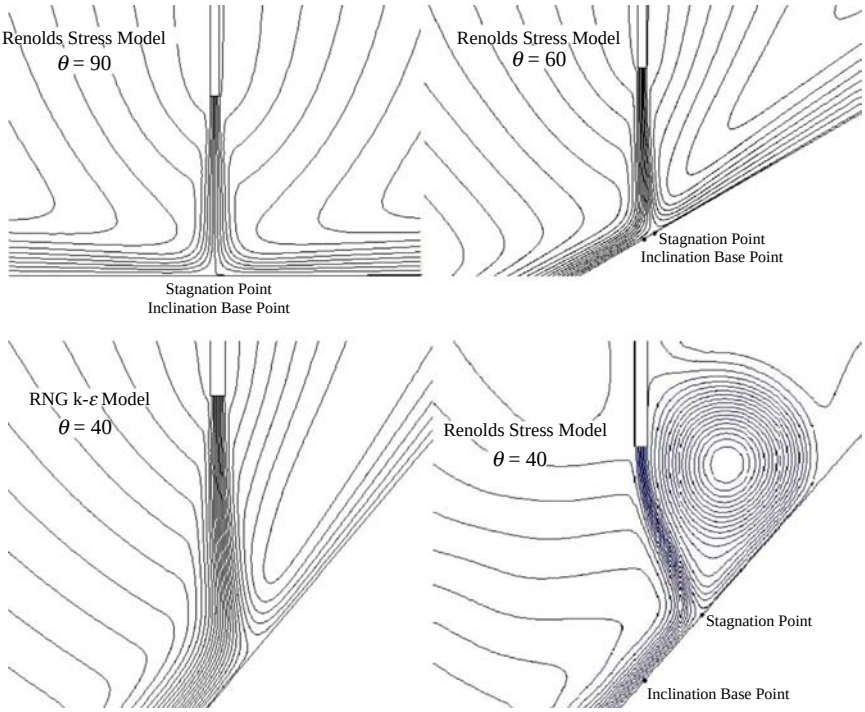

Figure 4.
Flow streamlines and creation of recirculation flow at $\theta = 40°$ ($H/D = 10$, $Re = 12{,}000$)

In a flat plate impinging jet, the inclination base point and stagnation point are at the same position. However, as the inclination angle decreases, the stagnation point moves to the uphill side of the plate and finally at $\theta = 40$ a recirculating flow is created between the uphill side of the plate on one side, and nozzle wall and nozzle exit streamlines on the other side. The effect of inclination on the downhill side of the inclined plate is a strengthening of the wall jet flow.

When only considering the flow field in an inclined impinging jet, Nusselt number value after the peak on the uphill side is expected to fall sharply. This is because of the wake flow and loss of momentum on the wall. However, on the downhill side, reduction of the Nusselt number happens gradually along the wall jet region.

The change in streamlines with respect to the Reynolds number is shown in Figure 5. The results illustrate a reduction in the size of recirculating flow at the uphill side of the plate as the Reynolds number increases. Finally, at $Re = 16{,}000$, the recirculating flow disappears. This is probably due to a stronger wall jet flow on the uphill side of the impinging plate as the Reynolds number increases. The streamlines also show slight movement of the stagnation point to the downhill side of the impinging plate as the Reynolds number increases.

Figure 6 shows the numerical prediction of the local Nusselt number of a flat plate impinging jet with constant $H/D = 6$ and dissimilar Reynolds numbers, and its comparison with experimental data (Beitelmal *et al.*, 2000). The trends of Nusselt number prediction by the Reynolds stress model in the impinging region and some parts of the wall jet regions show a better agreement with experiments while the RNG

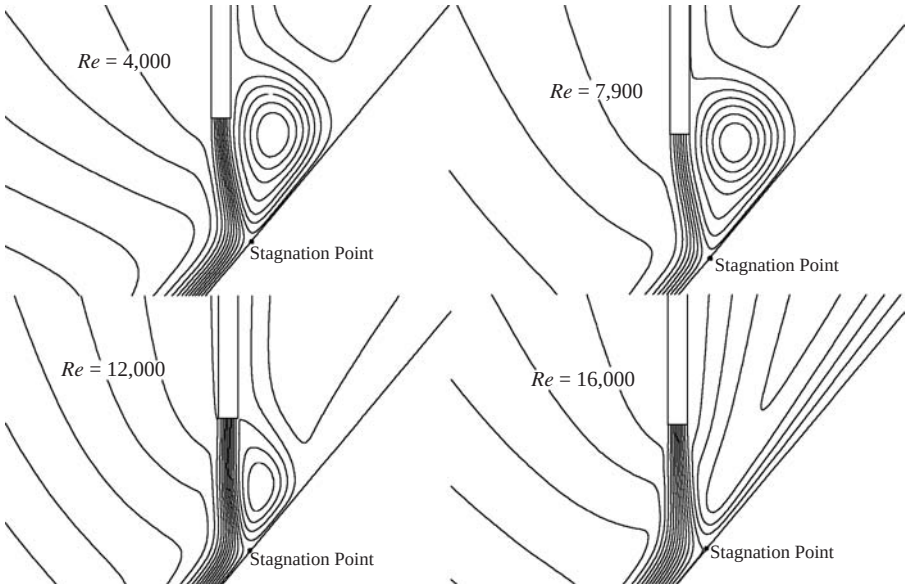

Figure 5.
Flow streamlines by Reynolds stress model and for different Reynolds numbers ($H/D = 6$, $\theta = 40°$)

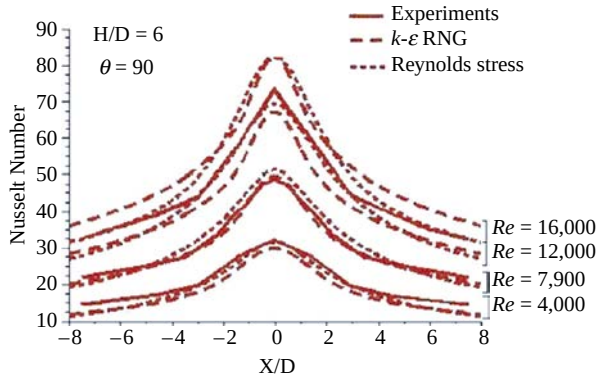

Figure 6.
Local Nusselt number on the flat plate impinging jet plate for different Reynolds numbers

k-ε model shows a sharper reduction from the maximum point. In the wall jet regions, the RNG k-ε model shows better trends compared to the Reynolds stress model that has a steeper heat transfer rate reduction. The experimental comparison of the Nusselt number at the stagnation point with the RNG k-ε model in the range of the Reynolds number studied shows less than 7 per cent variation whilst a maximum of 5 per cent variation was observed compared to the Reynolds stress model.

The results of different Reynolds numbers for an inclined impinging jet are shown in Figure 7. These results are for $H/D = 6$ and $\theta = 40$. As the results show, the trends of the RNG k-ε model are more reliable than the Reynolds stress model. In low inclination angle Reynolds stress model fails to predict trends of the local Nusselt number on uphill side of its peak. This can be seen as a sudden reduction of the Nusselt

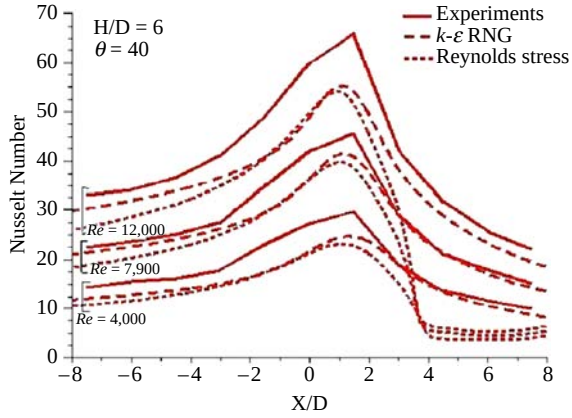

Figure 7.
Local Nusselt number on the inclined impinging jet plate for different Reynolds numbers

number in Figure 7. Moreover, the trends of the RNG k-ε model on downhill side shows a better agreement compared to experimental values. It should be noted that the reported experimental data are not for the Nusselt number peak location. Therefore, comparing the results of this study to that of experimental data has been carried out at $X/D = 1.5$ the nearest location to the peak. The results for the RNG k-ε model in the range of Reynolds numbers studied show a maximum of 15 per cent underestimation. A notable contribution of this study is to predict the exact peak location of the Nusselt number. This location was estimated by the RNG k-ε model for $Re = 4{,}000$, 7,900, 12,000 to be at $X/D = 1.32$, 1.14, and 1.00, respectively, and illustrates that decreasing of Reynolds number causes the peak Nusselt number location to move to the uphill side of the inclined plate. This is consistent with the movement of flow stagnation point with the Reynolds number (Figure 5).

The results of the heat transfer rate for an inclination angle $\theta = 70$, Reynolds number ($Re = 4{,}000$) and different values of H/D show more accurate prediction for the low H/D (Figure 8). The percentage difference between experimental values and numerical results of RNG k-ε and the Reynolds stress models are varied between 2.7 per cent in $H/D = 4$ and 16 per cent in $H/D = 8$ and 10. The maximum Nusselt number location for $H/D = 4$, 6, 8, and 10 by RNG k-ε model happens at $X/D = 0.28$, 0.34, 0.45, and 0.50, respectively, which shows the maximum heat transfer rate position moves more towards the uphill side with increasing value of the H/D.

Figure 9 shows the local Nusselt number on the inclined impinging plate with different inclination angles and two different H/D. The results show that the Reynolds stress model fails to predict trends of the local Nusselt number in a low inclination angle as shown in Figure 7. This failure for $H/D = 10$ in Figure 9 is coupled with extra movement of the maximum Nusselt number location to the uphill side of the inclined plate. The trends of the heat transfer rate obtained from RNG k-ε model in the stagnation region and along the inclined wall give a more accurate prediction. However, its value at the peak Nusselt number location for $H/D = 10$ is 20 per cent underestimated according to the experimental data. The comparison of the RNG k-ε model and experimental results shows approximately 5 per cent underestimation for

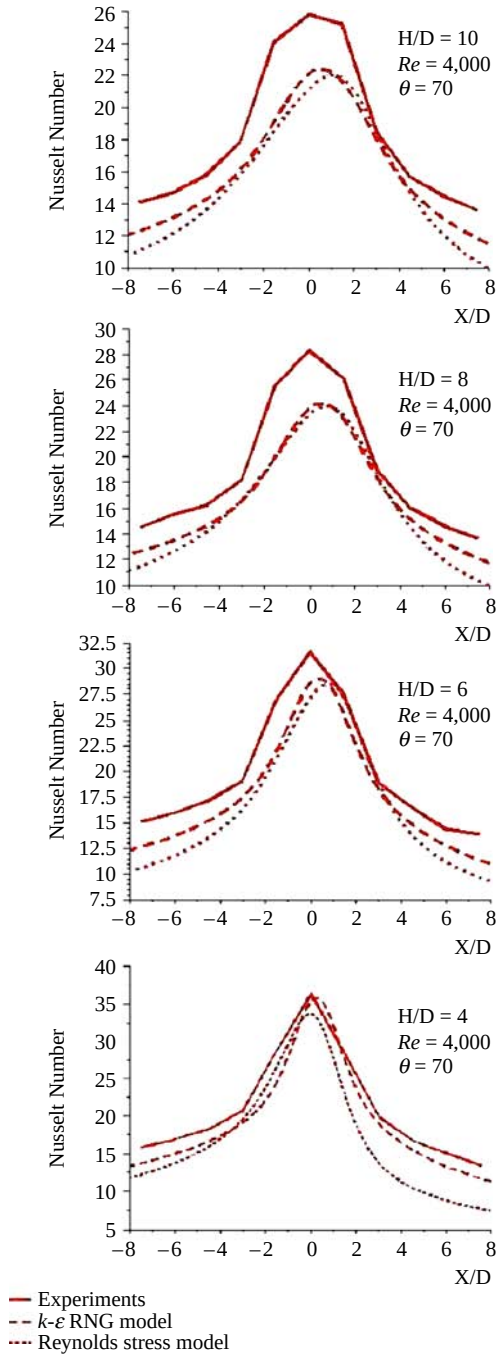

Figure 8.
Local Nusselt number on the inclined impinging jet plate for different *H/D*

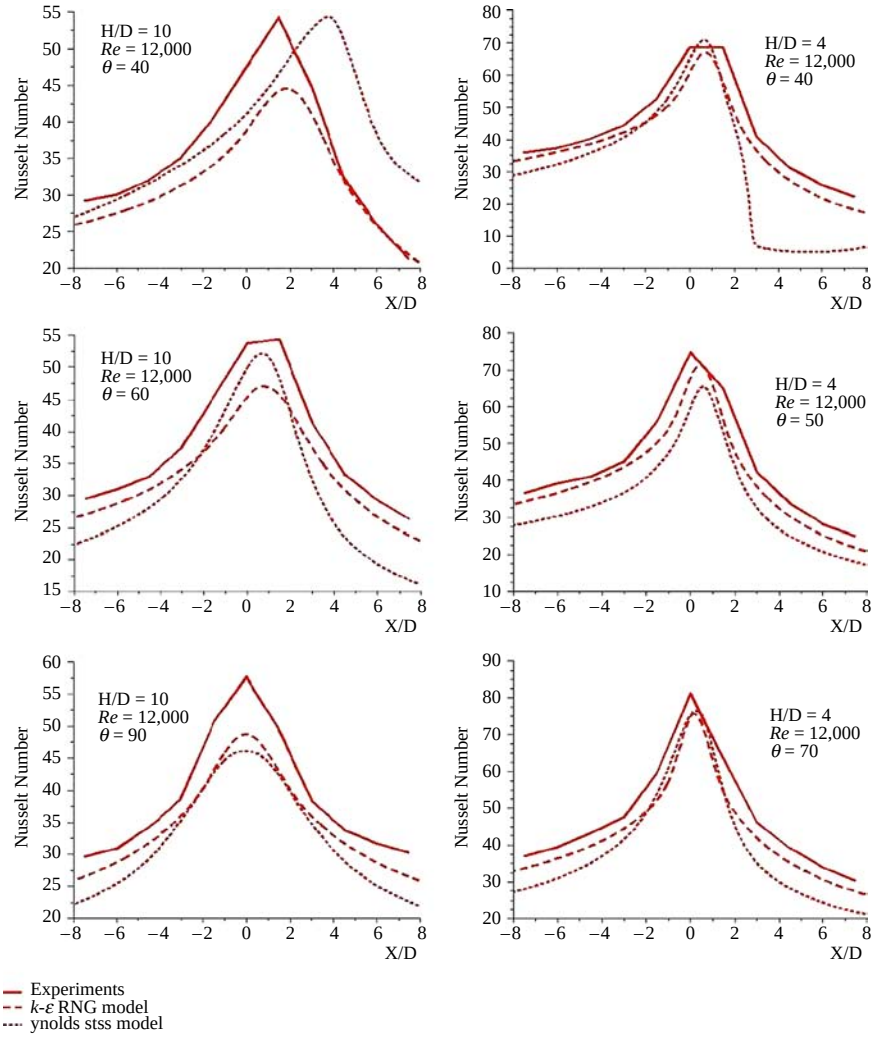

Figure 9.
Local Nusselt number on the inclined impinging jet plate for $H/D = 4$ and 10 and different inclination angles

the heat transfer rate close to the maximum Nusselt number location. The location of the peak heat transfer rate moves further to the uphill side of the inclined plate as the inclination angle decreases. The location of the maximum Nusselt number in Figure 9 for constant value $H/D = 10$ and $\theta = 90$, 60, and 40 estimated by the RNG k-ε model happens at $X/D = -0.02$, 0.78, and 1.85 and for constant value of $H/D = 4$ and $\theta = 70$, 50, 40 occurs at $X/D = 0.14$, 0.44, and 0.75, respectively. The value of the heat transfer rate by Reynolds stress model with different angles gives better results in comparison to the RNG k-ε model. However, the Reynolds stress model for the case of $\theta = 40$ fails to predict satisfactorily trends of the local Nusselt number at the uphill side of inclined impinging plate.

4. Conclusions

The numerical simulation was conducted to predict the local heat transfer rate on flat and inclined impinging jet plates by using the RNG k-ε and the basic Reynolds stress models with enhanced wall treatment for the near wall turbulence modelling. The value of the local Nusselt number for specified range of Reynolds number, H/D, and inclination angle was predicted within 1-20 per cent difference compared to the experimental values. This difference was increased at high values of H/D and slightly increased in low inclination angles. The trends of the local Nusselt number by applying the RNG k-ε model showed better prediction in the range of this study. However, the value of the Nusselt number was underestimated in a stagnation region in high H/D. The Reynolds stress model predicted the local Nusselt number value in lower inclination angles better than the RNG k-ε model apart from lowest angle in range of this study, $\theta = 40$. A notable contribution of this study is to predict the exact peak locations of the Nusselt number on inclined impinging plates as Reynolds number, H/D, and inclination angle change.

Generally, this study agrees with the reported previous studies that the Reynolds stress model leads to a more accurate prediction of flow field. However, the heat transfer rate at the wall strongly depends on the near wall turbulence modelling. The enhanced wall treatment showed satisfactory results in modelling the heat transfer rate of impinging jets. Furthermore, the RNG k-ε model with modified second constant in ε equation, leads to reduction of turbulence kinetic energy in a high-strain stagnation region.

References

Baughn, J. and Shimizu, S. (1989), "Heat transfer measurements from a surface with uniform heat flux and an impinging jet", *J. Heat Transfer*, Vol. 111, pp. 1096-8.

Behnia, M., Parneix, S. and Durbin, P. (1996), "Simulation for jet impingement heat transfer with the $k - \varepsilon - \overline{v^2}$ model", Annual Research Briefs, Centre for Turbulent Research, Stanford University, Stanford, CA, available at: http://ctr.stanford.edu/

Behnia, M., Parneix, S., Shabany, Y. and Durbin, P.A. (1999), "Numerical study of turbulent heat transfer in confined and unconfined impinging jets", *Int. J. Heat Fluid Flow*, Vol. 20, pp. 1-9.

Beitelmal, A.H., Saad, M.A. and Patel, C.D. (2000), "The effect of inclination on the heat transfer between a flat surface and an impinging two-dimensional air jet", *Int. J. Heat Fluid Flow*, Vol. 21, pp. 156-63.

Beltaos, S. (1976), "Oblique impingement of circular turbulent jets", *J. Hydraulic Research*, Vol. 14, pp. 17-36.

Craft, T.J., Graham, L.J.W. and Launder, B.E. (1993), "Impinging jet studies for turbulence model assessment-II. An examination of the performance of four turbulence models", *Int. J. Heat Mass Transfer*, Vol. 36, pp. 2685-97.

Durbin, P. (1995), "Separated flow computations with the $k - \varepsilon - \overline{v^2}$ model", *AIAA J.*, Vol. 33, pp. 659-64.

Durbin, P.A. (1996), "On the k-ε stagnation point anomaly", *Int. J. Heat Fluid Flow*, Vol. 17, pp. 89-90.

Fluent (2005), *FLUENT User's Guide*, Fluent Inc., Lebanon, NH.

Guerra, D.R.S., Su, J. and Silva Freire, A.P. (2005), "The near wall behaviour of an impinging jet", *Int. J. Heat Mass Transfer*, Vol. 48, pp. 2829-40.

Kader, B. (1981), "Temperature and concentration profiles in fully turbulent boundary layers", *Int. J. Heat Mass Transfer*, Vol. 24 No. 9, pp. 1541-4.

Lytle, D. and Webb, B. (1994), "Air jet impinging heat transfer at low nozzle-plate spacings", *Int. J. Heat Mass Transfer*, Vol. 37, pp. 1687-97.

Morris, G.K., Garimella, S.V. and Fitzgerald, J.A. (1999), "Flow-field prediction in submerged and confined jet impingement using the Reynolds stress model", *J. Electronic Packaging*, Vol. 121, pp. 255-62.

Obot, N., Mujumadar, A. and Douglas, W. (1982), "Effect of semi-confinement on impinging heat transfer", *Proceedings of 7th Int. Heat Transfer Conference*, Vol. 3, pp. 395-400.

Park, T.H., Choi, H.G., Yoo, J.Y. and Kim, S.J. (2003), "Streamline upwind numerical simulation of two-dimensional confined impinging slot jets", *Int. J. Heat Mass Transfer*, Vol. 46, pp. 251-62.

Park, T.S. and Sung, H.J. (2001), "Development of a near wall turbulence model and application to jet impingement heat transfer", *Int. J. Heat Fluid Flow*, Vol. 22, pp. 10-18.

Roy, S. and Patel, P. (2003), "Study of heat transfer for a pair of rectangular jets impinging on an inclined surface", *Int. J. Heat Mass Transfer*, Vol. 46, pp. 411-25.

Royne, A. and Dey, C.J. (2006), "Effect of nozzle geometry on pressure drop and heat transfer in submerged jet arrays", *Int. J. Heat Mass Transfer*, Vol. 49, pp. 800-4.

Saad, N.R., Polat, S. and Douglas, W.J.M. (1992), "Confined multiple impinging slot jets without crossflow effects", *Int. J. Heat Fluid Flow*, Vol. 13, pp. 2-14.

Sahoo, D. and Sharif, M.A.R. (2004), "Numerical modelling of slot-jet impingement cooling of a constant heat flux surface confined by a parallel wall", *Int. J. Thermal Science*, Vol. 43, pp. 877-87.

Stevens, J. and Webb, B.W. (1991), "The effect of inclination on local heat transfer under an axisymmetric free liquid jet", *Int. J. Heat Mass Transfer*, Vol. 34, pp. 1227-36.

Yan, X. and Saniei, N. (1997), "Heat transfer from an oblique impinging air jet to a flat plate", *Int. J. Heat Fluid Flow*, Vol. 18 No. 6, pp. 591-9.

Yue-Tzu, Y. and Yong-Xun, W. (2005), "Three-dimensional numerical simulation of an inclined jet with cross-flow", *Int. J. Heat Mass Transfer*, Vol. 48, pp. 4019-27.

Yung-Yang, S., Chin-Hao, H. and Ming-Hong, S. (1997), "Impingement cooling of a confined circular air jet", *Int. J. Heat Mass Transfer*, Vol. 40, pp. 1355-64.

Corresponding author
Ahad Ramezanpour can be contacted at: a.ramezanpour@anglia.ac.uk